Protective effect of phosphorylated Athyrium multidentatum (Doll.) Ching polysaccharide on vascular endothelial cells in vitro and in vivo

Kaiyue Yin
Weifang Medical University
Jiyu Chen
Weifang Medical University
Changqing Miao
Weifang Medical University
Feng Gao
Weifang Medical University
Jiwen Sheng
Weifang Medical University
Dongmei Liu (ldmwfmc@163.com)
Weifang Medical University

Research Article

Keywords: Phosphorylated polysaccharide, Vascular endothelial cell protection, RNA sequencing

Posted Date: April 18th, 2023

DOI: https://doi.org/10.21203/rs.3.rs-2796173/v1

Abstract

The purpose of this study was to prepare phosphorylated *Athyrium multidentatum* (Doll.) Cing polysaccharide (PPS) and investigate its protective effect on vascular endothelial cells (VECs) *in vitro* and *in vivo* and the underlying mechanisms. Sodium tripolyphosphate (STPP) and sodium trimetaphosphate (STMP) were used as phosphorylation reagents and PPS was characterized by Fourier transform infrared (FT-IR), ^{13}C nuclear magnetic resonance (^{13}C NMR) and ^{31}P nuclear magnetic resonance (^{31}P NMR) spectra. Chemical analysis demonstrated that PPS was composed of mannose, glucosamine, rhamnose, glucuronic acid, galacturonic acid, galactosamine, glucose, galactose, xylose, arabinose and fucose with a molar ratio of 11.36:0.42:4.03:1.12:1.81:0.26:33.25:24.12:6.85:14.46:2.32 and a molecular weight of 28837 Da. Results from *in vitro* and *in vivo* assays revealed that PPS protected human umbilical vein endothelial cells (HUVECs) against H_2O_2-induced oxidative injury and attenuated VECs damage in mice treated with D-galactose. RNA sequencing (RNA-seq) analysis disclosed that PPS down- or up-regulated the expression of eighteen differentially expressed genes (DEGs) involved in the functions of vascular endothelium repairment, cell growth and proliferation, cell survival and apoptosis, inflammation, angiogenesis and antioxidant in mice abdominal aorta, implying that these biological processes might play crucial roles in the protective actions of PPS on VECs.

Introduction

Cardiovascular disease (CVD) is a leading cause of death and disability globally [1]. It is generally associated with damages to arteries in organs such as brain, heart, eye and kidney. Vascular endothelial cells serve as not only a protective barrier on the surface of blood vessels but also an active source for the synthesis, metabolism, uptake, storage and degradation of multiple vasoactive substances [2]. Impairment of endothelial cells may trigger a significant decrease in blood flow and subsequent tissue damages in certain organs. Therefore, protecting VECs from damage is regarded as an essential strategy for CVD prevention.

Athyrium multidentatum (Doll.) Ching (AMC), a typical terrestrial fern with bearded rhizome and leaf blade ovate-lanceolate, is an ancient folk medicine used for hypertensive, rheumatisms and flu in Changbai Mountain area of China [3]. Polysaccharides from AMC were reported to possess excellent antioxidant, anti-aging, cytoprotective and immune-enhancing activities, denoting broad application prospects in the field of medicine, foods and health products [4–6]. In recent years, polysaccharides have aroused extensive attention of researchers because of their diverse biological activities and unique physical and chemical properties. Biological activities of polysaccharides are intimately related to several structure parameters such as molecular weight distributions, monosaccharide compositions and linkage types [7]. Structural modifications including methylation, sulfation, acetylation and phosphorylation can change the physicochemical and biological properties of polysaccharides and thus acquire better or unique activities [8]. Phosphorylation is considered as an effective covalent modification method that introduces the phosphate groups to the hydroxy groups of polysaccharides. Evidence had proved that the introduction of the phosphate groups may lead to better biological activities due to their high nucleophilic characteristic and remarkable hydrogen donation capacity. Deng et al. [9] reported that phosphorylated polysaccharides from *Dictyophora indusiata* displayed more powerful effects on the growth of MCF-7/B16 tumor cells than unmodified *Dictyophora indusiata polysaccharides*. Ye et al. [10] reported that polysaccharides from *Lachnum* YM120 had more excellent anti-tumor activity after phosphorylation. Our previous study suggested that phosphorylated AMC polysaccharide exhibited a potential protective effect on HUVECs. However, to the best of our knowledge, the phosphorylated polysaccharide of AMC was never investigated. Therefore, the protective effect of phosphorylated AMC polysaccharide on VECs *in vitro* and *in vivo* were explored in this study.

To achieve this objective, phosphorylated AMC polysaccharide was prepared by STPP-STMP method and characterized by monosaccharide composition, molecular weight, phosphorus content, FT-IR, ^{13}C NMR and ^{31}P NMR spectral analyses. Protective effect on VECs was evaluated employing H_2O_2-injured HUVECs and D-galactose-induced aging mice. RNA-seq analysis was applied to explore the underlying mechanisms and quantitative real-time reverse-transcription PCR (RT-qPCR) was performed to testify its reliability. Current study aimed to provide an experimental basis for the development and utilization of phosphorylated AMC polysaccharide as a novel vasoprotective agent.

Materials And Methods

Materials and reagents

Athyrium multidentatum (Doll.) Ching rhizome was harvested in Changbai Mountain area of China. Hyclone RPMI 1640 medium and mitochondrial membrane potential assay kit with JC-1 were purchased from Solarbio Science & Technology Co., Ltd (Beijing, China). Fetal bovine serum (FBS) was obtained from Sijiqing Biological Engineering Materials Co., Ltd (Hangzhou, China). Annexin V-FITC apoptosis detection kit was acquired from Becton, Dickinson and Company (New Jersey, USA). Superoxide dismutase (SOD), catalase (CAT) and glutathione peroxidase (GSH-Px) assay kits were obtained from Nanjing Jiancheng Bioengineering Institute (Nanjing, China). Reactive oxygen species (ROS) detection kit was purchased from Jiangsu Kaiji Biotech. Co., Ltd (Shanghai, China). Mouse enzyme linked immunosorbent assay (ELISA) kits were acquired from MultiSciences (Lianke) Biotech. Co., Ltd (Hangzhou, China). HiFiScript gDNA removal cDNA synthesis kit was purchased from ComWin Biotech. Co., Ltd (Beijing, China). SYBR® green realtime PCR master mix was acquired from Toyobo Co., Ltd (Osaka, Japan). Gene primers were synthesized by Jinan Ruizhi Biotech. Co., Ltd (Jinan, China). *In situ* cell death detection kit was obtained from Beyotime Biotech. Co., Ltd (Shanghai, China). H_2O_2, DMSO and vitamin E (VE) were acquired from Sigma Chemical Co. (St. Louis, MO, USA). Other chemicals were of analytical grade and purchased from Sinopharm Chemical Reagent Co., Ltd (Shanghai, China).

Preparation of phosphorylated polysaccharides

Polysaccharides from AMC were prepared according to the method described previously [6]. Briefly, 2.5 kg of AMC rhizomes were defatted with a 5-fold volume of methanol and then extracted with 18 L of distilled water at 100°C for 1.5 h twice. Afterwards, the water extract was concentrated and precipitated with a 3-fold volume of anhydrous ethanol. After filtering, the resultant precipitate was collected and extracted repeatly with a mixture of n-butanol and chloroform (1:4, v/v). The protein-free supernatant was dialyzed against tap water for 48 h and against distilled water for 24 h using 3500 Da Mw cutoff dialysis membranes to acquire AMC polysaccharides (PS). To prepare the phosphorylated polysaccharides, 5 g of PS was dissolved in a 500 mL mixture of 5% STPP and 2% STMP, and stirred at room temperature. After the solids were entirely dissolved, the pH value of the solution was adjusted to 9 with saturated $NaHCO_3$ solution and the mixture was allowed to react at 88°C for 5 h. At the end of reaction, the mixture was cooled to room temperature and precipitated with 3 times the volume of anhydrous ethanol. The resultant precipitant was redissolved in distilled water and dialyzed against tap water for 48 h and against distilled water for 48 h using 3500 Da Mw cutoff dialysis membranes. After lyophilization, phosphorylated AMC polysaccharide (PPS) was synthesized.

Structure characterization

Determination of phosphorus content

0.1091 g of polysaccharide sample was digested with a mixture of HNO_3 (5 mL), HCl (1 mL) and H_2O_2 (0.5 mL) at 25°C for 15 min and 200°C for 60 min. The obtained solution was subsequently diluted to 10 mL with distilled water. Measurement of phosphorus (P) content was carried out on an inductively coupled plasma mass spectrometer (ICP-MS, Aglient 7700, USA) under the conditions of carrier gas 1.10 L/min, omega bias − 105 V, omega lens 10.1 V, cell entrance − 45 V, deflect 3.8 V, cell exit − 62 V, plate bias − 60 V, RF power 1.50 KW and RF matching 1.80 V. A calibration curve was established by plotting the absorption intensities against the phosphorus concentrations (0, 5, 10, 25, 50 and 100 mg/L). Degree of substitution (DS) represented the average number of phosphate groups on each monosaccharide residue and was calculated according to the following formula, where P% standed for the phosphate group content.

$DS = (162 \times P\%)/(3100 - 84 \times P\%)$

Molecular weight determination

The molecular weights were achieved on a Shimadzu LC-20A HPLC system (Shimadzu Co., Kyoto, Japan) equipped with a TSK-GEL G3000 PWxl column (300 × 7.8 mm, 5 μm) and a refractive index detector. A 20 μL of sample solution was in each run and eluted with 0.1 mol/L Na_2SO_4 buffer at a flow rate of 0.5 mL/min. The molecular weight was estimated by reference to the calibration curve made from the T-series Dextran standards of known molecular weights (Mw 13.05, 36.80, 64.65, 135.35 and 300.60 kDa).

Monosaccharide composition analysis

The high performance liquid chiomatography (HPLC) method of pre-column derivatization with 1-phenyl-3-methyl-5-pyrazolone (PMP) was employed to determine the monosaccharide composition. In brief, 10 mg of polysaccharide sample was hydrolyzed with 1 mL of 4 mol/L trifluoroacetic acid (TFA) at 105°C for 4 h and then derivatized by 0.3 mol/L NaOH and 0.5 mol/L PMP at 70°C for 30 min.

After removal of residual PMP using chloroform, the solution was applied to a YMC-Pack ODS-AQ column (250 × 4.6 mm, 5 μm) connected to an Agilent 1260 HPLC system with a PDA detector (Agilent, USA). PBS (0.1 mol/L, pH 6.8) and acetonitrile (83:17, v/v) were used as mobile phase with a flow rate of 0.8 mL/min. Eleven monosaccharides, including mannose (Man), glucosamine (GlcN), rhamnose (Rha), glucuronic acid (GlcA), galacturonic acid (GalA), galactosamine (GalN), glucose (Glc), galactose (Gal), xylose (Xyl), arabinose (Ara) and fucose (Fuc), were used as standards.

Spectroscopic methods

The ultraviolet absorption spectra were measured on a UV-Vis spectrophotometer (UV-2700, Shimadzu, Japan) in the wavelength range 200–400 nm. Fourier transform infrared spectrophotometer (Shimadzu FTIR-8300) was used for IR spectrum analysis within the scanning area from 4000 to 400 cm^{-1} with a resolution of 4 cm^{-1}. The NMR spectra were recorded on a 500 MHz Bruker Avance III spectrometer equipped with a 5 mm multinuclear inverse detection probe, operating at 126 and 202 MHz for ^{13}C and ^{31}P nuclei, respectively. Here, samples were analyzed in deuterated dimethylsulfoxide (DMSO-d_6) reagent and the chemical shifs were given in parts per million (ppm).

Protective effect of phosphorylated polysaccharides on HUVECs

Cell culture

Human umbilical vein endothelial cells were donated by Institute of Plastic Surgery, Weifang Medical University (Weifang, China). Cells were propagated in sterile RPMI 1640 medium supplemented with 10% FBS and 1% penicillin-streptomycin mixture, and incubated in a humidified atmosphere containing 5% CO_2 at 37°C. After reaching 90–95% confluence, cells were passaged at a ratio of 1:2.

Cell proliferative rate

Cell proliferative rate was detected by CCK-8 method and all operations were performed according to the manufacturer's instructions. Briefly, cells were seeded at a density of 5×10^3 cells/well in a 96-well microplate and allowed to adhere for 12 h. Afterwards, cells were cocultured with 25, 50, 100 and 150 μg/mL polysaccharide samples or 10 μM VE for 24 or 48 h. At the end of treatment, 300 μM of H_2O_2 was added and incubated with the cells for another 50 min. Finally, 20 μL of CCK-8 was added and incubated with the cells for 4 h. The absorbance was measured at 450 nm on a SpectraMax M5 microplate reader (Molecular Devices Corporation, California, USA). The cell proliferative rate was calculated according to the following equation.

Cell proliferative rate (%) = $A_{sample\ 450}/A_{control\ 450} \times 100\%$

SOD/CAT/GSH-Px activities, MDA/NO contents and ROS level

Cells were seeded at a density of 1×10^5 cells/well in a 6-well plate. 12 h later, the cells were pretreated with 25, 50, 100 and 150 μg/mL polysaccharide samples or 10 μM VE for 48 h, and then exposed to 300 μM of H_2O_2 for 50 min. At the end of treatment, antioxidant enzymes (SOD, CAT and GSH-Px) activities and nitric oxide/malondialdehyde (NO/MDA) contents in the supernatants were respectively measured using a SpectraMax M5 microplate reader followed the manufacturer's protocols. 2',7'-Dichlorofluorescein diacetate (DCFH-DA) was used as a ROS capturing reagent. In brief, cells were seeded into a 96-well black plate at a density of 1×10^4 cells/well and cultured at 37°C for 12 h. Afterwards, 100 μL of different concentrations of polysaccharide solution (25, 50, 100 and 150 μg/mL) or VE (10 μM) was added and incubated at 37°C for 48 h. At the end of treatment, cell supernatant was abandoned and cells were exposed to DCFH-DA for 20 min. After rinsing with FBS-free 1640 medium twice, cells were exposed to 300 μM H_2O_2 for 50 min. The fluorescence intensity of DCF in cells was detected at an excitation wavelength of 488 nm and an emission wavelength of 525 nm using a SpectraMax M5 microplate reader. The intracellular ROS level was directly recorded as the fluorescent intensity.

Apoptosis analysis

Annexin V-FITC/PI double staining was performed to label apoptotic cells and the percentage of apoptotic cells was analyzed by flow cytometry. Briefly, cells were cultured at a density of 1×10^5 cells/well in a 6-well plate and allowed to attach for 12 h at 37°C. After cultivation with 150 μg/mL of polysaccharide samples or 10 μM of VE for 48 h, cells were treated with 300 μM of H_2O_2 for 50 min. Afterwards, cells were respectively stained with Annexin V-FITC and PI according to the manufacturer's instruction. Finally, the cells was analyzed by a Becton Dickinson FACS Calibur flow cytometer (BD Biosciences, San Jose, CA, USA).

Mitochondrial membrane potential

Assessment of mitochondrial membrane potential (MMP) was performed with the JC-1 reagent. Specifically, cells were seeded at a density of 1×10^5 cells/well in a 6-well plate and cultured at 37°C for 12 h. Afterwards, cells were pretreated with polysaccharide samples (150 μg/mL) or VE (10 μM) for 48 h and then exposed to 300 μM H_2O_2 for 50 min. At the end of treatment, cells were collected and stained with JC-1 following the manufacturer's protocols. Determination was performed on a Becton Dickinson FACS Calibur flow cytometer.

Protective effect of phosphorylated polysaccharides on VECs in D-galactose-induced aging mice

Experimental protocols

To implement *in vivo* assays, male Kunming mice weighing 26 ± 2 g (12-week-old) were purchased from Experimental Animal Center of Shandong Province, Jinan, China (Certificate No. SCXK 20140007). All mice were housed at 25 ± 2°C under a standard 12 h light/12 h dark cycle with *ad libitum* usage of food and water. After 3 days of acclimatization, the D-galactose-induced (100 mg/kg/day, ip) aging mice were divided randomly into five groups (16 mice per group), including: D-galactose model control group, positive control group (using VE as the positive drug, 200 mg/kg/day, ig), PPS low-dose group (50 mg/kg/day, ig), PPS medium-dose group (100 mg/kg/day, ig) and PPS high-dose group (200 mg/kg/day, ig). Another 16 healthy mice were selected as the normal control group. After 60 consecutive days of administration, mice were anesthetized and euthanized by cervical dislocation. The blood was collected by eyeball extraction and the abdominal aorta was meticulously excised and fixed in 4% paraformaldehyde for hematoxylin-eosin (HE) and TdT-mediated dUTP nick-end labeling (TUNEL) staining or kept in liquid nitrogen for RNA-seq and RT-qPCR assays.

HE and TUNEL staining

After fixing overnight, HE and TUNEL staining of the abdominal aorta was carried out. In brief, abdominal aorta was embedded in paraffin wax, sectioned at 5 μm thickness and stained with hematoxylin and eosin for microscopic observation under an Olympus BX51 light microscope (Olympus, Tokyo, Japan). TUNEL staining was conducted using an *in situ* cell death detection kit according to the manufacturer's recommendation. Five areas were selected randomly in each sample and the percentage of TUNEL-positive cells was calculated by Image J software.

Analysis of serum samples

The blood sample was stored at 4°C overnight and then centrifuged at 12000 rpm for 30 min at 4°C to separate the serum. The biomarkers, including SOD, CAT, GSH-Px, ROS, NO, endothelial nitric oxide synthase (eNOS), endothelin-1 (ET-1), tumor necrosis factor-α (TNF-α), interferon-γ (IFN-γ), interleukin-2 (IL-2), intercellular cell adhesion molecule-1 (ICAM-1), vascular cell adhesion molecule-1 (VCAM-1) and monocyte chemotactic protein-1 (MCP-1), were measured on a SpectraMax M5 microplate reader using commercially available test kits according to the manufacturer's instruction.

RNA-seq analysis

RNA-seq was performed to seek for target genes involved in the endothelial cell protective effect of PPS. Briefly, total RNAs of the model group and PPS high-dose group were isolated from the abdominal aorta tissues using Trizol reagent. The RNA purity and concentration were checked by a NanoPhotometer® spectrophotometer (IMPLEN, Westlake Village, CA, USA), and RNA integrity was measured using the Agilent RNA 6000 Nano Kit and a 2100 Bioanalyzer (Agilent Technologies, CA, USA). 1 μg of RNA was used to construct the sequencing libraries by employing the Illumina's TruSeq Small RNA Sample Prep Kit. After library profile analysis, the libraries were sequenced on an Illumina HiSeq × 10 platform (Annoroad Genomics, Beijing, China). The gene levels were quantified as fragments per kilobase of transcript per million mapped reads (FPKM) and normalized across all samples by the cuffdiff program. Gene Ontology (GO) function and Kyoto Encyclopedia of Genes and Genomes (KEGG) pathway enrichment analyses of the DEGs were performed with clusterProfiler package in R language. The $|\log_2 FC| \geq 1$ and adjusted *P* value of < 0.05 compared with the model group were adopted as standards to screen the DEGs.

RT-qPCR assay

RT-qPCR assay was implemented to testify the RNA-seq results. The total RNAs were extracted from abdominal aorta of mice by Trizol method. The concentration and purity of the isolated RNA were assessed according to the absorbance ratio at 260 and 280 nm with a NanoDrop one microvolume UV-Vis spectrophotometer from Thermo Fisher Scientific (USA). Total RNA was reverse-transcribed into

cDNA following the manufacturer's instruction. RT-qPCR was conducted on a 7500 Fast Dx real-time PCR instrument (Shanghai, China) adopting the procedures of 95°C for 30 s, 40 cycles at 95°C for 5 s, 55°C for 20 s and 72°C for 30 s. The sequences of primers applied to this study were listed in Table 1.

Table 1
Primer sequences used for RT-qPCR

Genes	Primer sequence (5'→3')	Tm (°C)	GC (%)
Klf6	F: GTTTCTGCTCGGACTCCTGAT	57.0	52.4
	R: TTCCTGGAAGALGCTACACATTG	54.6	43.5
Hspa1a	F: TGTGTATTGCACGTGGGCT	57.4	52.5
	R: GAAGGACCCGACACAAGCAT	57.9	55.0
Nr4a1	F: TTGAGTTCGGCAAGCCTACC	57.9	55.0
	R: GTGTACCCGTCCATGAAGGTG	58.4	57.1
Bct	F: AATTCTCCACTGTGTGGTAGCA	56.0	45.5
	R: GGTTTTCACTTTCTGTCTAGGGG	55.4	47.8
Nfkbiz	F: GCTCCGACTCCTCCGATTTC	58.4	60.0
	R: GAGTTCTTCACGCGAACACC	56.7	55.0
C5ar1	F: ATGGACCCCATAGATAACAGCA	55.3	45.5
	R: GAGTAGATGATAAGGGCTGCAAC	55.3	47.8
H2-Q10	F: GTGTTCAGGTCTCTCCTGTGA	56.4	52.4
	R: GGAGTTGGAAGGCTGACTGTA	56.7	52.4
GAPDH	F: AGGTCGGTGTGAACGGATTTG	62.6	52.4
	R: TGTAGACCATGTAGTTGAGGTCA	60.2	43.5

Statistical analysis

All experiments were performed in triplicate. The data were presented as means ± SDs and analyzed by one-way analysis of variance (ANOVA) followed by Dunnett's test using SPSS 17.0 software. A *P* value of less than *0.05* was considered statistically significant.

Results And Discussion

Chemical composition of phosphorylated polysaccharides

A total of 28.5 g of PPS was prepared from PS with a yield of 78%. As displayed in Table 2, the weight average molecular weight of PPS was estimated to be 28837 Da according to the calibration curve $f(x) = 0.001370995x^3 - 0.05493433x^2 + 0.3701789x + 6.138186$ ($R^2 = 0.9989526$), which was a bit lower than that of PS (30735 Da) (Supplementary Fig. S1). We conjectured that the phosphorylation reaction might have an impact on the molecular weight of polysaccharides. According to the regression equation $y = 718.5677x - 442.3883$ ($R^2 = 0.9998$), the phosphorus contents in PPS and PS were respectively calculated to be 7.71% and 0.06%, implying that the phosphorylated derivative of PS with a DS of 0.51 was prepared successfully. Monosaccharide composition analysis revealed that PPS and PS were composed of Man, GlcN, Rha, GlcA, GalA, GalN, Glc, Gal, Xyl, Ara and Fuc with molar ratios of 11.36:0.42:4.03:1.12:1.81:0.26:33.25:24.12:6.85:14.46:2.32 and 9.71:0.45:3.93:1.48:2.48:0.76: 39.11:20.78:7.92:11.70:1.69 (Supplementary Fig. S2), respectively. Obviously, glucose, galactose, arabinose, xylose and mannose were the major monosaccharide constituents, which was consistent with our results published previously [6].

Table 2
Molecular weights and chemical compositions of PPS and PS from *Athyrium multidentatum* (Doll.) Ching

Samples	Phosphorus content (%)	Molecular weight (Da)	Molar ratios										
			Man	GlcN	Rha	GlcA	GalA	GalN	Glc	Gal	Xyl	Ara	Fuc
PPS	7.71	28837	11.36	0.42	4.03	1.12	1.81	0.26	33.25	24.12	6.85	14.46	2.32
PS	0.06	30735	9.71	0.45	3.93	1.48	2.48	0.76	39.11	20.78	7.92	11.70	1.69

Spectroscopic characteristics

The nucleic acid and protein were monitored by UV absorption at 260 and 280 nm. As depicted in Fig. 1A, scanned UV spectra showed no absorption at 260 or 280 nm, manifesting that PS and PPS were nucleic acid and protein free. The profiles of the FT-IR spectra for PS and PPS were displayed in Fig. 1B. It could be seen that there were significant differences between the FT-IR spectra of PS and PPS. To be specific, the broad peaks appearing at around 3254.31 cm^{-1} and 2932.38 cm^{-1} vested in the characteristic absorption peaks of O–H and C–H stretching vibration. The bands at around 1722.49, 1602.89 and 1371.52 cm^{-1} were separately due to the asymmetric and symmetric vibration of –COOH, indicating that PS and PPS contained acidic polysaccharides, which was consistent with the result of monosaccharide composition analysis. The peaks near 1145.58 cm^{-1} and 926.91 cm^{-1} were ascribed to the characteristic absorption of carbohydrate. Compared with the FT-IR spectrum of PS, PPS showed a new characteristic absorption peak at 895.39 cm^{-1}, which was attributed to the symmetrical C-O-P vibration of C-O-PO_3 group [11]. Beyond that, the increment in the intensity of signal at 1240.14 cm^{-1} was corresponded to the stretching vibration of P = O [10, 12]. Current FT-IR analysis suggested that the phosphorylated modification of PS occurred successfully.

^{13}C NMR spectrum is usually applied to investigate the structure of polysaccharides, especially the phosphorylated position of polysaccharides. In present research, ^{13}C NMR and ^{31}P NMR spectra were applied together to establish the fingerprint profiles of PPS and PS. As shown in Fig. 1C, the ^{13}C NMR spectrum of PS displayed multiple peaks at 108.52, 103.98, 103.76, 103.34, 85.21, 83.71, 83.00, 81.31, 76.78, 76.19, 75.87, 75.34, 74.31, 73.98, 69.15, 63.72, 61.52, 61.19, 54.81, 47.80, 47.50, 47.20, 46.47 and 18.93 ppm. These chemical shifts were assigned according to the ^{13}C NMR data from literature. Correspondingly, signals at δ 103.76 (C-1), 76.78 (C-5), 76.19 (C-3), 73.98 (C-2), 69.15 (C-4) and 61.52 (C-6) ppm might be assigned to 1-β-D-Glc*p*- [13]. Resonances at δ 103.34 (C-1), 81.31 (C-4), 76.19 (C-5), 75.87 (C-3), 73.98 (C-2) and 61.52 (C-6) ppm were attributed to 1,4-β-D-Glc*p*- [14]. Signals at δ 103.98 (C-1), 69.15 (C-2), 83.00 (C-3), 63.72 (C-4), 75.34 (C-5) and 61.19 (C-6) ppm might belong to 1-β-D-Gal*p*-, and signals at δ 108.52 (C-1), 81.31 (C-2), 76.78 (C-3), 83.71 (C-4) and 61.19 (C-5) ppm were identified as 1-α-D-Ara*f*- [15]. Signals at δ 103.34 (C-1), 73.98 (C-2), 76.78 (C-3), 85.21 (C-4), 75.87 (C-5) and 63.72 (C-6) ppm might be ascribed to 1,x-β-D-Xyl*p*- [16]. Signals at δ 18.93 ppm pertained to the carbon of rhamnose methyl, confirming the presence of rhamnose. Previous methylation analysis revealed the existence of t-Glc*p*, 1,4-Glc*p*, t-Ara*f*, 1,x-Gal*p*, 1,x-β-D-Xyl*p*- and 1,2,4-Rha*p* residues in AMC polysaccharides [6], indicating a good correlation with current results. It is generally recognized that the carbon signal will shift towards lower field position if an electron-withdrawing phosphate group directly attaches to the carbon, while the signal will shift to higher field position if the phosphate group is indirectly connected [17, 18]. However, compared the carbon signals of PPS with that of PS, no significant induction occurred. We speculated that the hydroxyl groups of PS were not completely substituted. Encouragingly, three peaks at 17.28, 17.69 and 19.07 ppm emerged in the ^{31}P NMR spectrum of PPS (Fig. 1D), proclaiming the existence of phosphorus atoms from different phosphorylated positions in the glucosidic units. Taken together, phosphorylated AMC polysaccharides with high DS were prepared successfully.

Protective effect of phosphorylated polysaccharides on HUVECs

Effect of PPS on cell proliferation

The CCK-8 assay results revealed that the cell proliferative rates in the model group were respectively decreased to 51.8 ± 3.31% at 24 h and 52.3 ± 0.12% at 48 h after cells were exposed to H_2O_2 for 50 min (Fig. 2). After pretreatment with PPS for 24 or 48 h, the cell proliferative rate was enhanced and the dose-effect patterns were presented at concentrations ranging from 25 to 150 μg/mL. The cell proliferative rates in 100 and 150 μg/mL PPS-treated groups were respectively raised to 63.7 ± 6.87% and 73.2 ± 4.45% at 24 h, and 80.2 ± 2.46% and 99.9 ± 1.63% at 48 h with significant difference at $P < 0.05$ or $P < 0.01$ level, which were higher than the VE-treated

group (59.9 ± 5.64% at 24 h and 64.3 ± 7.38% at 48 h) and PS-treated group (78.9 ± 4.07% and 96.8 ± 4.32% at 48 h) [5]. Obviously, PPS displayed the most strongest cytoproliferative activity at the concentration of 150 μg/mL and the treatment time of 48 h. The results also suggested that PPS exhibited no harmful effects on HUVECs within the concentration ranges of 25–150 μg/mL. Therefore, the following *in vitro* assays were performed employing PPS at this optimum concentration and treatment time.

Effects of PPS on SOD, CAT and GSH-Px activities, and MDA, NO and ROS levels in HUVECs

Seen from Table 3, PPS had positive impacts on SOD, CAT and GSH-Px activities, and MDA, NO and ROS levels. Compared with the normal group, the activities of SOD, CAT and GSH-Px and the content of NO in the model group were decreased, while the levels of MDA and ROS were increased dramatically. In contrast, PPS pretreatment enhanced SOD, CAT and GSH-Px activities, raised NO content, and reduced MDA and ROS levels. PPS regulated the levels of SOD, CAT and ROS in concentration-dependent manners. These results demonstrated that PPS possessed significant antioxidant activity *in vitro*. In previous study, we found that PS failed to increase the activity of GSH-Px in HUVECs [5]. Comprehensive consideration of these results, PPS displayed more powerful effects on these biomarkers than PS and VE at 100 and 150 μg/mL.

Table 3
Effect of PPS on SOD, CAT, GSH-Px, MDA, NO and ROS in HUVECs. NG, normal group; MG, model group, cells treated with 300 μM H_2O_2 alone for 50 min; VE, positive control group, cells treated with 10 μM VE for 48 h and 300 μM H_2O_2 for 50 min; PPS1, PPS2, PPS3 and PPS4, cells respectively treated with 25, 50, 100 or 150 μg/mL PPS for 48 h and 300 μM H_2O_2 for 50 min. Compared with the normal group, $^{*}P< 0.05$, $^{**}P< 0.01$; compared with the model group, $^{\Delta}P< 0.05$, $^{\Delta\Delta}P< 0.01$

Samples	SOD activity (U/mL)	CAT activity (U/mL)	GSH-Px activity (U)	NO content (μmol/L)	MDA content (nmol/mL)	ROS intensity
NG	8.51 ± 0.28	1.06 ± 0.19	21.26 ± 0.79	0.043 ± 0.003	0.79 ± 0.07	168.83 ± 11.13
MG	5.35 ± 0.31*	0.51 ± 0.02*	8.77 ± 0.79**	0.030 ± 0.003*	1.31 ± 0.12*	240.07 ± 6.05**
VE	6.79 ± 0.18$^{*,\Delta}$	1.18 ± 0.06$^{*,\Delta}$	18.42 ± 0.91$^{\Delta}$	0.041 ± 0.002$^{*,\Delta}$	0.91 ± 0.07	184.63 ± 13.23$^{\Delta\Delta}$
PPS1	6.67 ± 0.33	0.74 ± 0.04	22.84 ± 1.48$^{*,\Delta}$	0.040 ± 0.004	0.87 ± 0.03$^{*,\Delta}$	235.25 ± 0.65
PPS2	7.87 ± 0.29$^{\Delta}$	1.15 ± 0.08$^{*,\Delta\Delta}$	15.78 ± 1.18	0.037 ± 0.005*	0.97 ± 0.03*	232.63 ± 3.40
PPS3	10.04 ± 0.54$^{**,\Delta\Delta}$	1.93 ± 0.04$^{*,\Delta}$	34.21 ± 3.29$^{*,\Delta\Delta}$	0.055 ± 0.003$^{**,\Delta\Delta}$	0.75 ± 0.07$^{\Delta}$	183.67 ± 11.38$^{*,\Delta}$
PPS4	11.75 ± 1.21$^{**,\Delta\Delta}$	2.33 ± 0.03$^{**,\Delta\Delta}$	52.63 ± 5.38$^{**,\Delta\Delta}$	0.046 ± 0.003$^{\Delta}$	0.63 ± 0.02$^{*,\Delta}$	165.35 ± 4.52$^{*,\Delta\Delta}$

Effect of PPS on cell apoptosis and MMP in HUVECs

In the apoptosis assay, HUVECs were intervened with 150 μg/mL PPS for 48 h. As depicted in Fig. 3A, cells treated with H_2O_2 alone exhibited higher apoptosis rate of 27.65 ± 1.06% ($P< 0.01$) than the normal group (14.03 ± 0.32%), implying that H_2O_2 induced apoptosis. After PPS pretreatment, the cell apoptosis rate was reduced to 17.60 ± 0.36% ($P< 0.05$, $P< 0.01$), which was lower than the VE-treated group (23.90 ± 1.27%, $P< 0.05$) and PS-treated group (18.3 ± 0.49%, $P< 0.05$) [5]. Obviously, PPS exerted a strong anti-apoptosis effect on H_2O_2-treated HUVECs.

Membrane-permeant JC-1 dye was used to estimate the mitochondrial membranes permeability of HUVECs in this study. From Fig. 3B, it could be seen that the MMP level was significantly reduced in H_2O_2-alone treated group (1.90 ± 0.28%, $P< 0.01$) compared to the normal group (9.65 ± 0.18%). After 48 h treatment with 150 μg/mL PPS, the positive staining rate of the cells was enhanced to 6.00 ± 0.56% ($P< 0.05$, $P< 0.01$), which was higher than the VE-treated group (4.8 ± 0.01%, $P< 0.05$). In previous study, we reported that the MMP level in PS treatment group was 4.10 ± 0.46% under the same conditions [5], which was lower than that of PPS treatment group, indicating that PPS was stronger than PS in enhancing MMP level.

Protective effect of phosphorylated polysaccharides on mice VECs

HE and TUNEL staining

The artery wall has a three-layered structure (intima, media and adventitia) governed the mechanical properties of vessels. Seen from the images of the abdominal aorta depicted in Fig. 4A, the artery wall of the normal group displayed a compact structure. The intima was smooth and covered with intact endothelial cells. The smooth muscle cells were in fusiform shape and regularly arranged in the media. The elastic membranes were intact, flabby, clear and continuous. After the mice were treated with D-galactose, the smooth muscle cells shrinked apparently and some cells appeared apoptosis. The elastic membranes turned straight and even ruptured. The media of the artery wall was loosely organized and many endothelial cells seemed to peel off the intima. A comparative analysis showed that PPS at a dosage of 100 mg/kg exhibited the most powerful protective effect on the abdominal aorta, which was stronger than VE. In short, PPS pretreatment presented significant ameliorations in D-galactose-induced mice abdominal aorta injuries, including increased smooth muscle and endothelial cells, flappy and intact elastic membranes, and tight artery wall structure, which could be clearly observed in the HE staining images.

TUNEL staining enables researchers to visualize and quantify cells undergoing apoptosis. In this assay, the apoptotic cells in the abdominal aorta were stained brown and the living cells were stained blue. As displayed in Fig. 4B, the cell apoptosis rates in the nomal group and the D-galactose-treated group were respectively 4.8 ± 0.12% and 78.1 ± 5.46%, indicating that D-galactose induced cell apoptosis in artery wall, which was consistent with the HE staining results. After administration of PPS at a dosage of 50 mg/kg, the apoptosis rate was decreased to 3.2 ± 0.31%. Inspiringly, the apoptotic cells were not observed in 100 and 150 mg/kg PPS treatment groups, which was similar to the VE treatment group. All things considered, PPS exhibited marked anti-apoptosis capacity, which agreed with our cell apoptosis results *in vitro*. We concluded that the decrease in cell apoptosis might be one of the potential protection mechanisms of PPS on vascular endothelial cells.

Effect of PPS on the activities of SOD, CAT and GSH-Px and the levels of ROS, NO, eNOS and ET-1 in mice serum

Similar to the *in vitro* experimental results, PPS showed powerful effects on the activities of SOD, CAT and GSH-Px as well as the levels of NO, eNOS and ROS *in vivo* (Table 4). Compared with the normal group, the activities of SOD, CAT and GSH-Px were attenuated in the model group. Reversely, PPS markedly enhanced the antioxidant enzyme activities in mice serum. Except for CAT in PPS1 group, the antioxidant enzymes activities in PPS treatment groups were stronger than the normal group and the CAT and GSH-Px activities were increased in dose-dependent manners. In comparison with VE, PPS had a more robust influence on the antioxidant enzyme activities. Meanwhile, the ROS levels in PPS-treated groups were lower than the model group and a dose-dependent manner was displayed. NO, the strongest diastolic vascular factor, has multiple functions including platelet aggregation prevention, neutrophil activation inhibition, anti-inflammatory and anti-apoptotic effects, and plays a crucial role in maintaining the balance of circulation and modulating the vascular tone [19]. The generation of the endothelial NO in VECs mainly depends on the activity of eNOS, which functions as a pivotal enzyme in the synthesis of NO. In this assay, NO and eNOS contents in the serum were minimized after the mice were treated with D-galactose. After intervention with PPS, the NO and eNOS levels were elevated, indicating its powerful protective effects on VECs. Oddly, a reversed dose-response relationship was presented in the NO levels. We concluded that NO migh be inhibited by PPS due to its increased antioxiant capacity at high concentrations since NO belonged to the reactive oxygen species. ET-1, a strong vasoconstrictor secreted by endothelial cells, acts as the natural counterpart of NO. The dynamic balance between NO and ET-1 plays an important role in instructing the normal tension of blood vessels [20]. Our results showed that the ratios of NO/ET-1 in the NG, MG, VE, PPS1, PPS2 and PPS3 groups were respectively 0.45, 0.23, 0.24, 0.60, 0.52 and 0.34, suggesting that PPS could effectively ameliorate vasomotor function. Therefore, the antioxidative activity and the regulating capacity on NO/ET-1 balance could probably contribute to the protective effect of PPS on VECs *in vivo*.

Table 4

Effect of PPS on SOD, CAT, GSH-Px, ROS, NO, eNOS and ET-1 in mice serum. NG, normal group; MG, model group, mice treated with D-galactose alone (100 mg/kg/day, ip) for 60 days; VE, positive control group, mice treated with VE (200 mg/kg/day, ig) and D-galactose (100 mg/kg/day, ip) for 60 days; PPS1, PPS2 and PPS3, mice respectively treated with 50, 100 or 200 mg/kg/day PPS (ig) and D-galactose (100 mg/kg/day, ip) for 60 days. Compared with the normal group, $^{*}P< 0.05$, $^{**}P< 0.01$; compared with the model group, $^{\Delta}P < 0.05$, $^{\Delta\Delta}P< 0.01$

Groups	SOD activity (U/mL)	CAT activity (U/mL)	GSH-Px activity (U/L)	ROS intensity	NO content (μmol/L)	eNOS content (pg/mL)	ET-1 content (pg/mL)
NG	74.15 ± 2.74	88.27 ± 12.21	1611.00 ± 71.14	551781 ± 811.05	10.21 ± 1.26	1108.55 ± 41.71	22.50 ± 1.74
MG	71.14 ± 3.23*	63.82 ± 7.50**	1523.34 ± 51.52*	588296 ± 763.21*	7.02 ± 0.58*	973.87 ± 51.42*	28.83 ± 3.43*
VE	73.37 ± 2.98$^{\Delta}$	47.69 ± 2.22	1559.77 ± 32.20	358131 ± 456.87**,$^{\Delta\Delta}$	5.88 ± 1.26*,$^{\Delta}$	1201.60 ± 19.21**,$^{\Delta}$	24.11 ± 3.10*,$^{\Delta}$
PPS1	74.29 ± 4.43	67.16 ± 9.72*	1616.70 ± 109.48$^{\Delta}$	559475 ± 425.90*	14.12 ± 2.07*,$^{\Delta\Delta}$	1035.53 ± 79.33	23.40 ± 3.63*,$^{\Delta}$
PPS2	76.35 ± 2.49*,$^{\Delta}$	92.75 ± 15.34*,$^{\Delta\Delta}$	1726.65 ± 77.93*,$^{\Delta}$	436450 ± 382.61*,$^{\Delta}$	11.65 ± 4.54*,$^{\Delta}$	1098.76 ± 19.07$^{\Delta}$	22.36 ± 1.90$^{\Delta}$
PPS3	76.27 ± 1.92*,$^{\Delta}$	104.03 ± 14.71*,$^{\Delta\Delta}$	1855.79 ± 445.08**,$^{\Delta\Delta}$	330466 ± 339.18**,$^{\Delta\Delta}$	8.25 ± 0.95*	1137.58 ± 54.25*,$^{\Delta}$	24.49 ± 2.59*,$^{\Delta}$

Effect of PPS on the levels of TNF-α, IFN-γ, IL-2, ICAM-1, VCAM-1 and MCP-1 in mice serum

In this study, the biomarkers including TNF-α, IFN-γ, IL-2, ICAM-1, VCAM-1 and MCP-1 in the mice serum were monitored. Seen from Table 5, IFN-γ, ICAM-1, VCAM-1 and MCP-1 levels were increased, while IL-2 levels were decreased in D-galactose-induced mice, implying that D-galactose triggered inflammatory injury. In contrast, PPS ameliorated endothelial damage through elevating IL-2 level or by lessening TNF-α, IFN-γ, ICAM-1, VCAM-1 and MCP-1 levels. The IFN-γ, IL-2 and ICAM-1 contents were in dose-dependent manners.

Table 5

Effect of PPS on TNF-α, IFN-γ, IL-2, ICAM-1, VCAM-1 and MCP-1 in mice serum. NG, normal group; MG, model group, mice treated with D-galactose alone (100 mg/kg/day, ip) for 60 days; VE, positive control group, mice treated with VE (200 mg/kg/day, ig) and D-galactose (100 mg/kg/day, ip) for 60 days; PPS1, PPS2 and PPS3, mice respectively treated with 50, 100 or 200 mg/kg/day PPS (ig) and D-galactose (100 mg/kg/day, ip) for 60 days. Compared with the normal group, $^{*}P< 0.05$, $^{**}P< 0.01$; compared with the model group, $^{\Delta}P< 0.05$, $^{\Delta\Delta}P< 0.01$

Groups	TNF-α (pg/mL)	IFN-γ (pg/mL)	IL-2 (pg/mL)	ICAM-1 (μg/mL)	VCAM-1 (μg/mL)	MCP-1 (pg/mL)
NG	501.44 ± 47.26	166.33 ± 17.97	14.31 ± 2.56	30.84 ± 3.11	1795.22 ± 149.69	468.88 ± 35.35
MG	498.56 ± 59.94	250.96 ± 16.86*	11.55 ± 4.10*	32.79 ± 4.65*	2130.00 ± 122.98**	487.63 ± 67.08*
VE	496.63 ± 20.83	51.38 ± 18.86**,$^{\Delta\Delta}$	11.64 ± 4.48*,$^{\Delta}$	33.42 ± 7.14$^{\Delta}$	1853.91 ± 153.72*,$^{\Delta}$	325.13 ± 33.63*,$^{\Delta}$
PPS1	438.94 ± 32.93*,$^{\Delta}$	174.29 ± 22.99*,$^{\Delta}$	10.60 ± 3.81	30.93 ± 3.98$^{\Delta}$	1552.83 ± 55.34**,$^{\Delta\Delta}$	418.88 ± 58.15$^{\Delta}$
PPS2	450.48 ± 46.46*	102.83 ± 33.72*,$^{\Delta\Delta}$	12.01 ± 2.00	30.69 ± 2.93$^{\Delta}$	1719.13 ± 118.70$^{\Delta}$	381.38 ± 37.50*,$^{\Delta\Delta}$
PPS3	477.88 ± 65.35*,$^{\Delta}$	62.21 ± 20.86**,$^{\Delta\Delta}$	13.07 ± 4.86*,$^{\Delta}$	29.55 ± 3.73*,$^{\Delta}$	1553.91 ± 43.04**,$^{\Delta\Delta}$	415.75 ± 57.73*,$^{\Delta}$

Effect of phosphorylated polysaccharides on genes in mice abdominal aorta

RNA sequencing assay

Genes corresponding to the protective actions of PPS were identified by RNA-seq analysis. As displayed in the volcano plots (Fig. 5A), a total of 175 DEGs (105 upregulated and 70 downregulated, Supplementary Fig. S3) were identified from PPS-treated abdominal aorta. Among these DEGs, eighteen DEGs might be contributed to the protective effect of PPS owing to their involvement in the functions of anti-oxidant, anti-apoptosis, anti-inflammation, promoting proliferation and stimulating angiogenesis and repair (Table 6). GO analysis is a useful method for annotating genes and gene sets with biological characteristics for highthroughput genome or transcriptome data. The upregulated and downregulated genes correlated with the protective actions of PPS were respectively involved in the biological processes of immune system process, cell proliferation, cellular process, reproductive process, biological adhesion, developmental process, growth, response to stimulus and biological regulation in the GO terms (Fig. 5B). The KEGG pathway is a knowledge base for systematic analysis of gene functions [21]. As shown in the KEGG barplot (Fig. 5C), MAPK (mitogen-activated protein kinase) signaling pathway might be responsible for the protective capacity of PPS, in which Nr4a1 (nuclear receptor subfamily 4, group a, member 1), Hspa1a (heat shock protein family a (Hsp70) member 1a), Dusp1 (dual specificity phosphatase 1) and Jun were involved (Supplementary Fig. S4). However, other KEGG pathways or signaling pathways seemed not to be intimately associated with the protective actions of PPS.

Table 6
Differentially expressed genes associated with the protective effect of PPS on vascular endothelial cells

DEGs	Up/down regulation	Functions
Klf6	up	repair damaged vascular endothelium
Kit	up	promote cell growth and proliferation
Nr4a1	up	promote cell survival, anti-apoptosis and induce angiogenesis
Nr4a3	up	promote apoptosis
Nfkbiz	up	promote cell survival and growth, anti-apoptosis
C5ar1	down	anti-vasculitis
Jun	up	promote angiogenesis
H2-Q10	up	antioxidant and scavenge free radicals
Btc	up	promote cell proliferation
Dusp1	up	anti-inflammation
Hspa1a	up	protect against cellular inflammation, apoptosis and oxidative stress
Hapa1b	up	protect against endothelial cell apoptosis
Errfi1	up	anti-inflammation and reduce the production of the inflammatory factors
Btg2	up	anti-proliferation
Ucp2	down	promote apoptosis
Ddah1	up	promote NO production
Tnfrsf10b	up	promote apoptosis
Sfrp5	up	reduce endothelial cell apoptosis

RT-qPCR analysis

Lastly, RT-qPCR was conducted to validate the DEGs identified in the RNA-seq analysis. The mRNA expression levels of Klf6 (Krüppel-like factor 6), Nr4a1, Nfkbiz (nuclear factor of kappa light polypeptide gene enhancer in B-cells inhibitor, zeta), Hspa1a, H2-Q10 and Btc (betacellulin) in the abdominal aorta were respectively examined in this assay. As displayed in Table 7, the mRNA expression levels of Klf6, Nr4a1, Nfkbiz, Hspa1a and H2-Q10 were significantly downregulated in the model group, whereas the expression of Btc mRNA was similar to the normal group. The expression levels of these genes were upregulated after the mice were administered with

50, 100 or 200 mg/kg PPS, which was entirely consistent with the RNA-seq results. Apart from Nr4a1 in PPS1 group and Btc in PPS3 group, the mRNA expression levels of the genes in PPS-treated groups were higher than the VE-treated group. A dose-dependent manner was observed in the transcription levels of Nr4a1. At a dosage of 100 mg/kg, PPS exhibited marked effects on Klf6, Hspa1a, H2-Q10 and Btc genes. All things considered, PPS exerted anti-oxidative, anti-inflammatory and anti-apoptotic activities by regulating the expression of the genes associated with cell apoptosis, cell proliferation, inflammation, anti-oxidant and so forth.

Table 7

Effect of PPS on the gene expression levels in mice abdominal aorta. NG, normal group; MG, model group, mice treated with D-galactose alone (100 mg/kg/day, ip) for 60 days; VE, positive control group, mice treated with VE (200 mg/kg/day, ig) and D-galactose (100 mg/kg/day, ip) for 60 days; PPS1, PPS2 and PPS3, mice respectively treated with 50, 100 or 200 mg/kg/day PPS (ig) and D-galactose (100 mg/kg/day, ip) for 60 days. Compared with the normal group, $^{*}P < 0.05$, $^{**}P < 0.01$; compared with the model group, $^{\Delta}P < 0.05$, $^{\Delta\Delta}P < 0.01$

Groups	Klf6	Nr4a1	Nfkbiz	Hspa1a	H2-Q10	Btc
NG	1.00 ± 0.21	1.00 ± 0.11	1.00 ± 0.12	1.00 ± 0.08	1.00 ± 0.12	1.00 ± 0.14
MG	0.76 ± 0.31	0.58 ± 0.74*	0.33 ± 0.005*	0.41 ± 0.20	0.23 ± 0.22*	1.11 ± 0.42
VE	3.97 ± 1.17$^{*,\Delta}$	3.02 ± 2.17$^{*,\Delta}$	3.72 ± 0.37*	3.02 ± 0.52$^{*,\Delta}$	3.22 ± 0.98$^{*,\Delta}$	2.91 ± 0.24$^{\Delta}$
PPS1	4.23 ± 1.88$^{*,\Delta}$	1.78 ± 0.09$^{\Delta}$	6.94 ± 3.93$^{*,\Delta}$	7.78 ± 2.74$^{*,\Delta}$	4.36 ± 2.00$^{*,\Delta}$	5.26 ± 0.07$^{*,\Delta}$
PPS2	431.63 ± 45.61$^{**,\Delta\Delta}$	4.44 ± 2.49$^{*,\Delta}$	6.46 ± 3.21$^{*,\Delta}$	203.85 ± 6.78$^{**,\Delta\Delta}$	58.09 ± 6.49$^{**,\Delta\Delta}$	159.32 ± 15.56$^{**,\Delta\Delta}$
PPS3	31.66 ± 9.18$^{**,\Delta\Delta}$	10.71 ± 0.72$^{**,\Delta\Delta}$	4.09 ± 0.69$^{*,\Delta}$	50.47 ± 5.60$^{**,\Delta\Delta}$	9.96 ± 0.81$^{**,\Delta\Delta}$	2.42 ± 0.62*

Degree of substitution is believed to have a great influence on the bioactivity of phosphorylated polysaccharides. However, the phosphorylated modification was very difficult to accomplish owing to the tough esterification process between -PO_4 and -OH and the complicated structures of polysaccharides. Multifarious phosphorylation reagents, including phosphoric acid, phosphorous acid, phosphonopropionic acid and tripolyphosphate, have been employed to prepare the phosphorylated polysaccharides. It is believed that phosphorus content and DS are closely associated with the types and ratios of phosphorylation reagents and/or the reaction conditions. Wang et al. [11] synthesized phosphorylated *Artemisia sphaerocephala* polysaccharides with a DS of 0.34–0.54 by $POCl_3$/pyridine technique. Here, STPP and STMP were proved to be convenient and efficient phosphorylation reagents owing to the desirable DS and mild reaction conditions.

Oxidative damages are associated with the pathogenesis of many chronic diseases, including atherosclerosis, stroke, chronic inflammatory diseases, cancers and degenerative diseases [22]. ROS-induced oxidative damage has distinct physiological and pathophysiological impacts on vascular cells. NO is an important cellular signaling molecule involved in many physiological and pathological processes. It can act directly on VECs and smooth muscle cells to activate guanylyl cyclase, which relaxes blood vessels through elevated cGMP [23]. In this assay, PPS increased antioxidative enzyme activities, promoted NO production and attenuated MDA and ROS levels, exerting strong antioxidative and cytoprotective activities. Phosphate groups enable polysaccharides to become excellent hydrogen atom donors through activating the hydrogen atom of the anomeric carbon, thus enhancing the antioxidant activities of polysaccharides [24]. Song et al. [25] reported that phosphorylated pumpkin polysaccharide exhibited relevant higher antioxidant activities and cytoprotective effects both *in vitro* and in a cell system than unmodified polysaccharide. Moreover, the introduced phosphate groups can trigger electrostatic effect and change the chain conformation of polysaccharides, leading to improved antioxidant activities. Phosphorylated garlic polysaccharide exhibited more powerful hydroxyl radical scavenging effect than unmodified garlic polysaccharide owing to the change in the molecular structure [26]. Hence, we conjectured that the introduction of phosphate groups contributed to the enhanced antioxidant activities of PPS, which migh play a key role in the protective actions of PPS towards VECs.

Apoptosis is an accurately controlled, energy-dependent process of cell death, normally occuring during the development and aging. It is considered as an essential homeostatic mechanism that maintains cell populations in tissues [27]. However, excessive apoptosis may gradually lead to the loss of the target-cell population and its effector functions [28]. Accumulating evidence has revealed that

ROSmediated oxidative stress is a key inducer of cell apoptosis. Our results suggested that PPS attenuated the apoptosis of vascular endothelial cells induced by H_2O_2 and D-galactose *via* suppressing ROS overproduction. Atherosclerosis is closely related to the development of cardiovascular diseases and the endothelial cell apoptosis is the first step of atherosclerosis [29]. Therefore, PPS might have great potential to ameliorate atherosclerosis due to its capacity of minimizing endothelial cell apoptosis. Mitochondrial membrane potential is a key indicator of mitochondrial activity because it reflects the process of electron transport and oxidative phosphorylation, and the driving force behind ATP production [30]. The dissipation of MMP constitutes an early irreversible step in the cascade of events leading to apoptosis [31]. Mitochondria disfunction may lead to decreased MMP and excessive ROS, and thus induce apoptosis [32]. Therefore, chemical constituents that contribute to enhance the level of MMP may lessen ROS generation and protect VECs from oxidative damage or apoptosis. PPS treatment led to the increase of SOD, CAT and GSH-Px activities and the decrease of ROS levels in HUVECs and mice serum, which might contribute to the augmentation of MMP levels and the ensuing reduction in apoptosis. Das et al. [33] found that nitrones protected endothelial cells against oxidative stress by modulating phase II antioxidant enzymes and subsequently inhibiting mitochondria-dependent apoptotic cascade, which was similar to our results.

Endothelial cell injury is a critical event in acute inflammatory processes, during which inflammatory cytokines and reactive oxygen metabolites may be involved [34]. TNF-α is a potent inflammatory cytokine leading to the expression and release of various inflammatory cytokines, chemokines and adhesion molecules necessary for the recruitment and migration of monocytes to the vessel intima [35], which are regarded as major markers of endothelial cell inflammatory damage. IFN-γ, a soluble cytokine produced by T lymphocytes, macrophages, mucosal epithelial cells or NK cells, plays central roles in the fundamental immunological processes such as inflammatory reaction, cell-mediated immunity and autoimmunity. Aberrant IFN-γ expression is intimately associated with multiple human diseases [36]. It was reported that TNF-α and IFN-γ treatment promoted distinct expression of the endothelial surface makers (selectins, ICAM-1 and VCAM-1) [37]. Here, PPS exerted benificial effects on endothelial cells by abating the secretion of inflammatory cytokines and cell adhesion molecules susceptible to damage the endothelial cells, directly. In light of the *in vivo* and *in vitro* data, PPS did protect VECs against damages owing to its properties of antioxidant, anti-inflammation, anti-apoptosis and functions of stimulating cell proliferation, promoting NO secretion and inhibiting ET-1 generation, which might play important roles in the protective actions of PPS on VECs.

Endothelial dysfunction is an important pathological mechanism for the development of atherosclerosis and can be triggered and deteriorated by a cluster of cardiometabolic risk factors, thereby provoking oxidative stress, infammation, cell cycle arrest or apoptosis in the endothelial cells [38]. Anti-oxidation and anti-inflammation interventions are considered to be the most effective strategies to inhibit endothelial cell damage and accelerate the recovery of endothelium functions so as to prevent the occurrence and development of atherosclerosis. In this experiment, RNA-seq analysis revealed up- or down-regulation of the proliferation-related genes Kit, Btc and Btg2 (B-cell translocation gene 2), antioxidative genes H2-Q10 and Hspa1a, cell apoptosis and survival-related genes Nr4a1, Nr4a3 (nuclear receptor subfamily 4, group a, member 3), Nfkbiz, Ucp2 (uncoupling protein 2), Hapa1b (heat shock protein family a (Hsp70) member 1b), Tnfrsf10b (tumor necrosis factor receptor superfamily, member 10b) and Sfrp5 (secreted frizzled-related protein 5), inflammation-related genes C5ar1 (complement component 5a receptor 1), Dusp1 and Errfi1 (ERBB receptor feedback inhibitor 1), and angiogenesis, repairment and NO production-related genes Jun, Klf6 and Ddah1 (dimethylarginine dimethylaminohydrolase 1) after PPS treatment. However, the most enriched KEGG pathway analysis found no network or cross-talk between these genes. We conjectured that PPS might exert its cytoprotective activity by directly regulating the expression of these genes.

H2-Q10, a fully reduced form of coenzyme Q10 (ubiquinol), has robust anti-oxidant and free radical scavenger effects and is widely used in clinic for cardiovascular and cerebrovascular diseases, nervous system diseases, hypertension, diabetes and so on [39]. In current study, the increased endogenous enzymes including SOD, CAT, GSH-Px and H2-Q10 contributed to the antioxidative effect of PPS. Dusp1, a negative regulator of the MAPK signaling pathway, is involved in various cellular responses including inflammation, cell proliferation, differentiation, apoptosis, stress responses and immune defense [40]. It was reported that Dusp1 participates in the regulation of hypoxia-induced RAW264.7 macrophage inflammatory and immune response by modulating the expression and the secretion of TNF-α, IL-10 and IL-1β [41]. Likewise, Errfi1 plays an important role in lessening inflammation, apoptosis and proliferation. The expression of Errfi1 prevented the proliferation and pro-inflammatory cytokine (IL-6, TNF-α, and IL-1β) production in nucleus pulposus cells [42]. We suggested that the decreased TNF-α levels in mice serum might be related to the overexpression of Dusp1 and Errfi1 in response to PPS treatment. The anti-apoptosis effect of PPS on VECs might also be mediated by the up-regulated genes Nr4a1, Hspa1a, Hapa1b, Nfkbiz, Sfrp5 and down-regulated gene Ucp2. To our surprise, the up-regulation of pro-apoptosis genes Tnfrsf10b and Nr4a3 ocurred concurrently, similar to the proliferation-related genes between Kit and Btc/Btg2. The existence of these paradoxical genes seemed to prevent VECs from excessive proliferation or apoptosis. In addition, genes such as Jun, Klf6 and Ddah1

might also have important impacts on the protective activity of PPS. Current results from biomarker determination, MMP and apoptosis measurement, HE/TUNEL staining and RNA-seq analysis stated that PPS was a powerful multi-target protective agent against VECs oxidative stress damage.

Conclusions

To sum up, PPS displayed significant anti-oxidation, anti-inflammation and anti-apoptosis activities *in vitro* and *in vivo*, implying its powerful protective capacity on VECs. The DEGs, including Klf6, Kit, Nr4a1, Nr4a3, Nfkbiz, C5ar1, Jun, H2-Q10, Btc, Dusp1, Hspa1a, Hapa1b, Errfi1, Btg2, Ucp2, Ddah1, Tnfrsf10b and Sfrp5, contributed to the protective effect of PPS on VECs. In light of the involvement of these genes in the functions of damaged vascular endothelium repairment, cell growth and proliferation, cell survival and apoptosis, inflammation, antioxidant, NO production inducement and angiogenesis, the molecular mechanisms underlying the protective effect of PPS might be characterized by synergistic effects of multi-targets. The phosphorylation modification of AMC polysaccharides provided us with a novel polysaccharide derivative having more active and potential as prevention and treatment drugs for cardiovascular disease.

Declarations

Ethical approval

This article does not contain any studies with human participants and all animal experiments were approved by the ethics committee of Weifang Medical University.

Competing interests

The authors declare that there are no conflicts of interest.

Author's contributions

Jiwen Sheng and Dongmei Liu wrote the main manuscript text, Kaiyue Yin and Jiyu Chen performed the experiments and prepared figures 1-5, Changqing Miao and Feng Gao prepared Table 1-7. All authors reviewed the manuscript.

Funding

This work was supported by the Natural Science Foundation of Shandong province (ZR2020MH402).

Availability of data and materials

All data and materials are available from the first and corresponding authors on reasonable request.

References

1. Mc Namara, K., Alzubaidi, H., Jackson, J.K.: Cardiovascular disease as a leading cause of death: how are pharmacists getting involved? Integr. Pharm. Res. Pract. **8**, 1–11 (2019)
2. Berridge, B.R., Van Vleet, J.F., Herman, E.: Chap. 46-Cardiac, vascular, and skeletal muscle systems. In: Haschek, W.M., Rousseaux, C.G., Wallig, M.A. (eds.) Haschek and Rousseaux's Handbook of Toxicologic Pathology, pp. 1567–1665. Elsevier Inc., New York (2013)
3. Liu, D.M., Sheng, J.W., Wang, S.H., Zhang, W.F., Zhang, X.H., Wang, D.Y.: Chemical constituents from *Athyrium multidentatum* (Doell.) Ching rhizome and their reducing power. Chin. J. Exp. Tradit Med. Formul. **22**(21), 185–188 (2016)
4. Jing, L., Jiang, J.R., Liu, D.M., Sheng, J.W., Zhang, W.F., Li, Z.J., Wei, L.Y.: Structural characterization and antioxidant activity of polysaccharides from *Athyrium multidentatum* (Doll.) Ching in D-galactose-induced aging mice *via* PI3K/AKT pathway. Molecules. **24**(18), 3364 (2019)
5. Jing, L., Sheng, J.W., Jiang, J.R., Wang, Y., Shen, X.Y., Liu, D.M., Zhang, W.F., Mao, S.M.: Chemical characteristics and cytoprotective activities of polysaccharide fractions from *Athyrium multidentatum*. (Doll.) Ching. Int. J. Biol. Macromol. **158**, 1227–1238 (2020)

6. Wang, Y., Shen, X.Y., Yin, K.Y., Miao, C.Q., Sun, Y.L., Mao, S.M., Liu, D.M., Sheng, J.W.: Structural characteristics and immune-enhancing activity of fractionated polysaccharides from *Athyrium multidentatum* (Doll.) Ching. Int. J. Biol. Macromol. **205**, 76–89 (2022)
7. Zhang, N., Qiu, S.Y., Mo, L.P., Wang, W.P., Wu, Y.G.: Optimization of processing of phosphorylated lentinan. Sci. Tech. Food Ind. **29**, 185–187 (2008)
8. Ge, Q., Zhang, A.Q., Sun, P.L.: Research progress in structural modifications of polysaccharide in fungi and their identification. Edible Fungi Chn. **27**(1), 5–9 (2008)
9. Deng, C., Fu, H.T., Xu, J.J., Shang, J.Y., Cheng, Y.M.: Physiochemical and biological properties of phosphorylated polysaccharides from *Dictyophora indusiata*. Int. J. Biol. Macromol. **72**, 894–899 (2015)
10. Ye, M., Yuan, R.Y., He, Y.L., Du, Z.Z., Ma, X.J.: Phosphorylation and anti-tumor activity of exopolysaccharide from *Lachnum* YM120. Carbohydr. Polym. **97**(2), 690–694 (2013)
11. Wang, J.L., Wang, Y.X., Xu, L., Wu, Q.Q., Wang, Q., Kong, W.B., Liang, J.Y., Yao, J., Zhang, J.: Synthesis and structural features of phosphorylated *Artemisia sphaerocephala* polysaccharide. Carbohydr. Polym. **181**, 19–26 (2018)
12. Kim, H.S., Song, M., Lee, E.J., Shin, U.S.: Injectable hydrogels derived from phosphorylated alginic acid calcium complexes. Mat. Sci. Eng. C-Mater. **51**, 139–147 (2015)
13. Suárez, E.R., Kralovec, J.A., Grindley, T.B.: Isolation of phosphorylated polysaccharides from algae: the immunostimulatory principle of *Chlorella pyrenoidosa*. Carbohydr. Polym. **345**(9), 1190–1204 (2010)
14. Dai, H., Han, X.Q., Gong, F.Y., Dong, H., Tu, P.F., Gao, X.M.: Structure elucidation and immunological function analysis of a novel beta-glucan from the fruit bodies of *Polyporus umbellatus* (Pers.) Fries. Glycobiol. **22**(12), 1673–1683 (2012)
15. Breitmaier, E., Voelter, W.: Carbon-13 NMR-spectroscopy, third completely rev. ed. VCH. New York (1987)
16. Yin, J.Y., Li, C., Nie, S.P., Xie, M.Y.: Structural characterization of purified polysaccharide fraction (PLP-1) from the seeds of *Plantago asiatica* L. Chem. J. Chin. Univ. **34**(12), 2728–2733 (2013)
17. Chen, Y., Zhang, H., Wang, X.Y., Nie, S.P., Li, C., Xie, M.Y.: Sulfated modification of the polysaccharides from *Ganoderma atrum* and their antioxidant and immunomodulating activities. Food Chem. **186**(1), 231–238 (2014)
18. Chen, T., Zhu, L., Liu, X.Y., Li, Y.Y., Zhao, C.D., Xu, Z.G., Yan, W.F., Zhang, H.X.: Synthesis and antioxidant activity of phosphorylated polysaccharide from *Portulaca oleracea* L. with $H_3PW_{12}O_{40}$ immobilized on polyamine functionalized polystyrene bead as catalyst.J. Mol. Catal. A-Chem. 342–343,74–78(2011)
19. Yao, L., Lu, P., Li, Y.M., Yang, L.J., Feng, H.X., Huang, Y., Zhang, D.D., Chen, J.G., Zhu, D.L.: Osthole relaxes pulmonary arteries through endothelial phosphatidylinositol 3-kinase/Akt-eNOS-NO signaling pathway in rats. Eur. J. Pharmacol. **699**, 23–32 (2013)
20. Zhu, J.Q., Song, W.S., Xu, S.X., Ma, Y., Wei, B.Y., Wang, H.W., Hua, S.Y.: Shenfu injection promotes vasodilation by enhancing eNOS activity through the PI3K/Akt signaling pathway *in vitro*. Front. Pharmacol. **11**, 121 (2020)
21. Kanehisa, M., Goto, S.: KEGG: Kyoto encyclopedia of genes and genomes. Nucleic Acids Res. **28**(1), 27–30 (2000)
22. Halliwell, B., Grootveld, M.: The measurement of free radical reactions in humans. Some thoughts for future experimentation. FEBS Lett. **213**(1), 9–14 (1987)
23. Archer, S.L., Huang, J.M., Hampl, V., Nelson, D.P., Shultz, P.J., Weir, E.K.: Nitric oxide and cGMP cause vasorelaxation by activation of a charybdotoxin-sensitive K channel by cGMP-dependent protein kinase. Proc. Natl. Acad. Sci. U. S. A. 91(16), 7583–7587 (1994)
24. Hu, H.B., Li, H.M., Han, M.H., Cao, Q., Liang, H.P., Yuan, R.N., Sun, J., Zhang, L.L., Wu, Y.: Chemical modification and antioxidant activity of the polysaccharide from *Acanthopanax leucorrhizus*. Carbohyd Res. **487**, 107890 (2019)
25. Song, Y., Ni, Y.Y., Hu, X.S., Li, Q.H.: Effect of phosphorylation on antioxidant activities of pumpkin (*Cucurbita pepo*, Lady godiva) polysaccharide. Int. J. Biol. Macromol. **81**, 41–48 (2015)
26. Chen, J.F., Huang, G.L.: Antioxidant activities of garlic polysaccharide and its phosphorylated derivative. Int. J. Biol. Macromol. **125**, 432–435 (2019)
27. Norbury, C.J., Hickson, I.D.: Cellular responses to DNA damage. Annu. Rev. Pharmacol. Toxicol. **41**, 367–401 (2001)
28. Brunner, T., Mueller, C.: Apoptosis in disease: About shortage and excess. Essays Biochem. **39**, 119–130 (2003)
29. Duan, H.X.Y., Zhang, Q., Liu, J., Li, R.L., Wang, D., Peng, W., Wu, C.J.: Suppression of apoptosis in vascular endothelial cell, the promising way for natural medicines to treat atherosclerosis. Pharmacol. Res. **168**, 105599 (2021)

30. Lee, Y.X., Lin, P.H., Rahmawati, E., Ma, Y.Y., Chan, C., Tzeng, C.R.: Chap. 20-Mitochondria Research in Human Reproduction. In: Leung, P.C.K., Adashi, E.Y. (eds.) The Ovary, pp. 327–335. Elsevier Inc., New York (2019)
31. Zamzami, N., Marchetti, P., Castedo, M., Zanin, C.: Reduction in mitochondrial potential constitutes an early irreversible step of programmed lymphocyte death *in vivo*. J. Exp. Med. **181**(5), 1661–1672 (1996)
32. Suski, J.M., Lebiedzinska, M., Bonora, M., Pinton, P., Duszynski, J., Wieckowski, M.R.: Relation between mitochondrial membrane potential and ROS formation. Methods Mol. Biol. **810**, 183–205 (2012)
33. Das, A., Gopalakrishnan, B., Voss, O.H., Doseff, A.I., Villamena, F.A.: Inhibition of ROS-induced apoptosis in endothelial cells by nitrone spin traps *via* induction of phase II enzymes and suppression of mitochondria-dependent pro-apoptotic signaling. Biochem. Pharm. **84**(4), 486–497 (2012)
34. Yamaoka, J., Kabashima, K., Kawanishi, M., Toda, K.I., Miyachi, Y.: Cytotoxicity of IFN-gamma and TNF-alpha for vascular endothelial cell is mediated by nitric oxide. Biochem. Biophys. Res. Commun. **291**(4), 780–786 (2002)
35. Zhang, H., Park, Y., Wu, J., Chen, X., Lee, S., Yang, J., Dellsperger, K.C., Zhang, C.: Role of TNF-alpha in vascular dysfunction. Clin. Sci. **116**(3), 219–230 (2009)
36. Ding, H.H., Wang, G.F., Yu, Z., Sun, H.M., Wang, L.: Role of interferon-gamma (IFN-γ) and IFN-γ receptor 1/2 (IFNγR1/2) in regulation of immunity, infection, and cancer development: IFN-γ-dependent or independent pathway. Biomed. Pharmacother. **155**, 113683 (2022)
37. Jaczewska, J., Abdulreda, M.H., Yau, C.Y., Schmitt, M.M., Schubert, I., Berggren, P.O., Weber, C., Koenen, R.R., Moy, V.T., Wojcikiewicz, E.P.: TNF-α and IFN-γ promote lymphocyte adhesion to endothelial junctional regions facilitating transendothelial migration. J. Leukoc. Biol. **95**, 265–274 (2014)
38. Sun, H.J., Wu, Z.Y., Nie, X.W., Bian, J.S.: Role of endothelial dysfunction in cardiovascular diseases: The link between inflammation and hydrogen sulfide. Front. Pharmacol. **10**, 1568 (2019)
39. Grammenandi, K., Kyriazi, M., Katsarou-Katsari, A., Papadopoulos, O., Anastassopoulou, I., Papaioannou, G.T., Sagriotis, A., Rallis, M., Maibach, H.I.: Low-molecular-weight hydrophilic and lipophilic antioxidants in nonmelanoma skin carcinomas and adjacent normal-looking skin. Skin. Pharm. Physiol. **29**, 324–331 (2016)
40. Peng, H.Z., Yun, Z., Wang, W., Ma, B.A.: Dual specificity phosphatase 1 has a protective role in osteoarthritis fibroblastlike synoviocytes *via* inhibition of the MAPK signaling pathway. Mol. Med. Rep. **16**(6), 8441–8447 (2017)
41. Dong, H.P., Liu, B., Zhang, E.L., Gao, Y.Q.: Expression of dual specificity phosphatase-1 in hypoxic RAW264.7 cells and its role in inflammatory immune response regulation. J. Third Mil Med. Univ. **42**(6), 560–567 (2020)
42. Guo, Y.S., Tian, L.J., Liu, X., He, Y.X., Chang, S.T., Shen, Y.: ERRFI1 inhibits proliferation and inflammation of nucleus pulposus and is negatively regulated by miR-2355-5p in intervertebral disc degeneration. Spine (Phila Pa 1976). **44**(15), E873–E881 (2019)

Figures

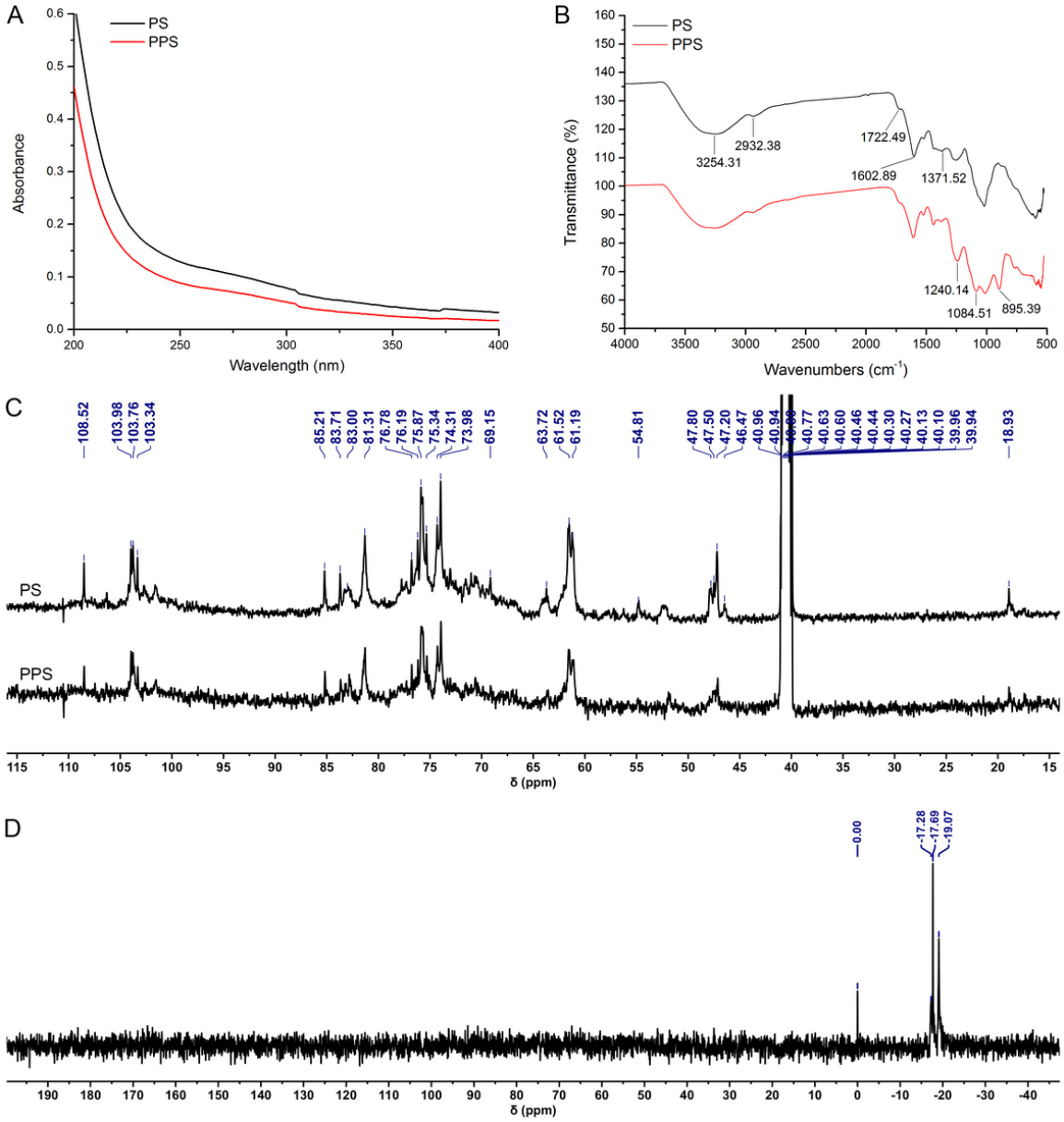

Figure 1

UV (A), FT-IR (B), ^{13}C NMR (C) and ^{31}P NMR (D) spectra of PPS and PS

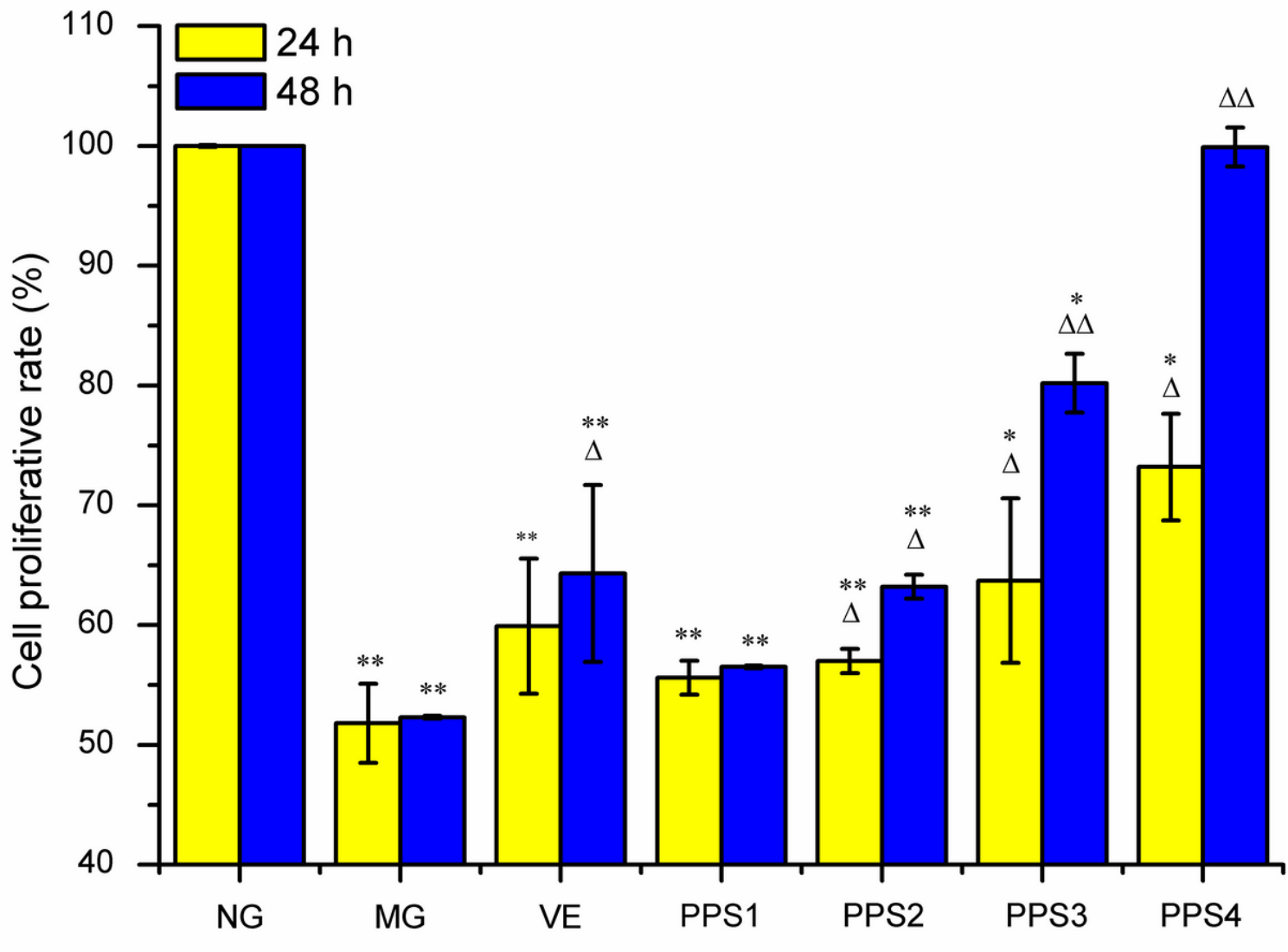

Figure 2

Effect of PPS on cell proliferation. NG, normal group; MG, model group, cells treated with 300 μM H_2O_2 alone for 50 min; VE, positive control group, cells treated with 10 μM VE for 48 h and 300 μM H_2O_2 for 50 min; PPS1, PPS2, PPS3 and PPS4, cells respectively treated with 25, 50, 100 or 150 μg/mL PPS for 48 h and 300 μM H_2O_2 for 50 min. Compared with the normal group, $^{*}P < 0.05$, $^{**}P < 0.01$; compared with the model group, $^{\Delta}P < 0.05$, $^{\Delta\Delta}P < 0.01$

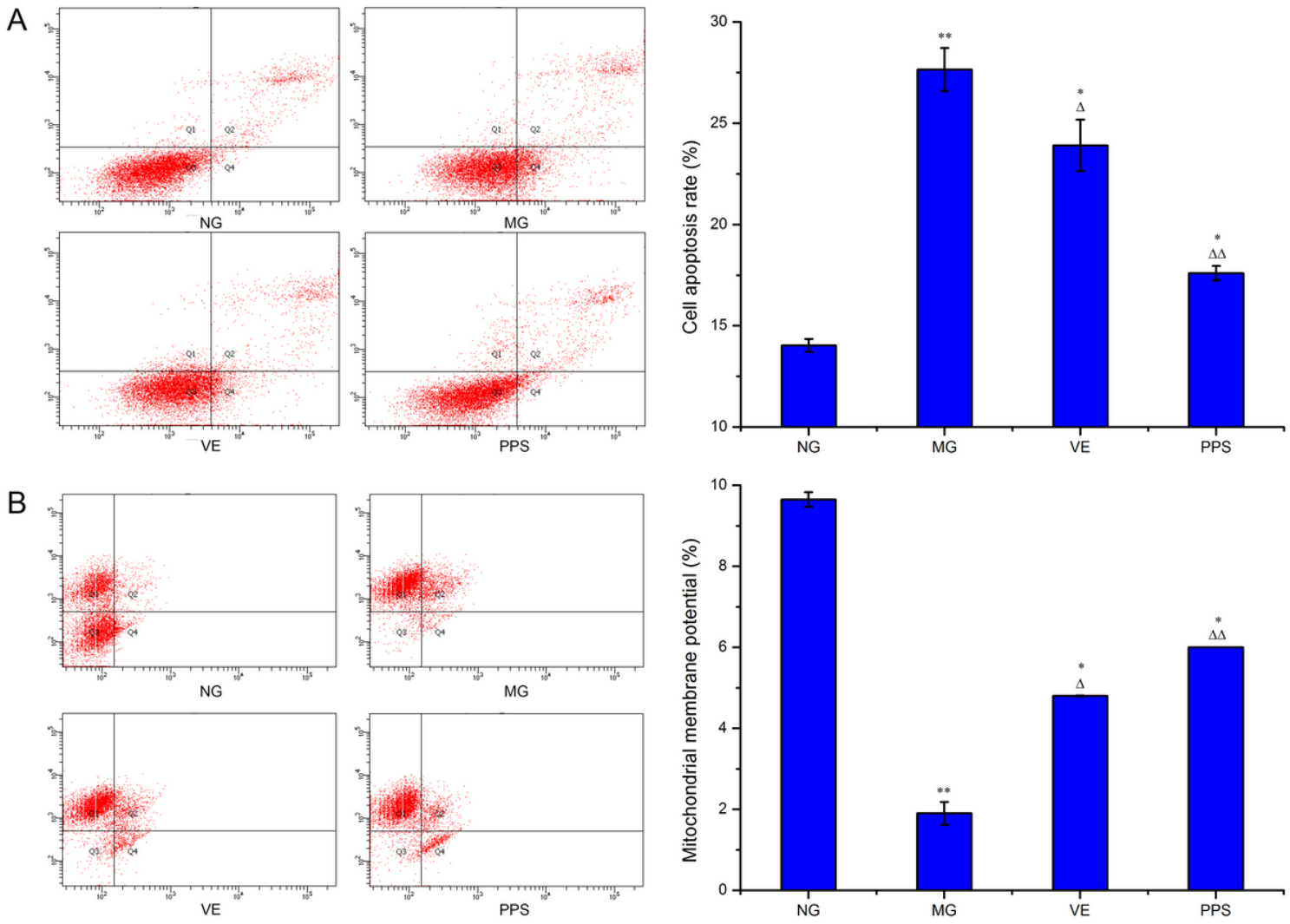

Figure 3

Apoptosis (A) and MMP (B) analyses of HUVECs by flow cytometry. NG, normal group; MG, model group, cells treated with 300 μM H_2O_2 alone for 50 min; VE, positive control group, cells treated with 10 μM VE for 48 h and 300 μM H_2O_2 for 50 min; PPS, cells treated with 150 μg/mL PPS for 48 h and 300 μM H_2O_2 for 50 min. Compared with the normal group, $^{*}P < 0.05$, $^{**}P < 0.01$; compared with the model group, $^{\Delta}P < 0.05$, $^{\Delta\Delta}P < 0.01$.

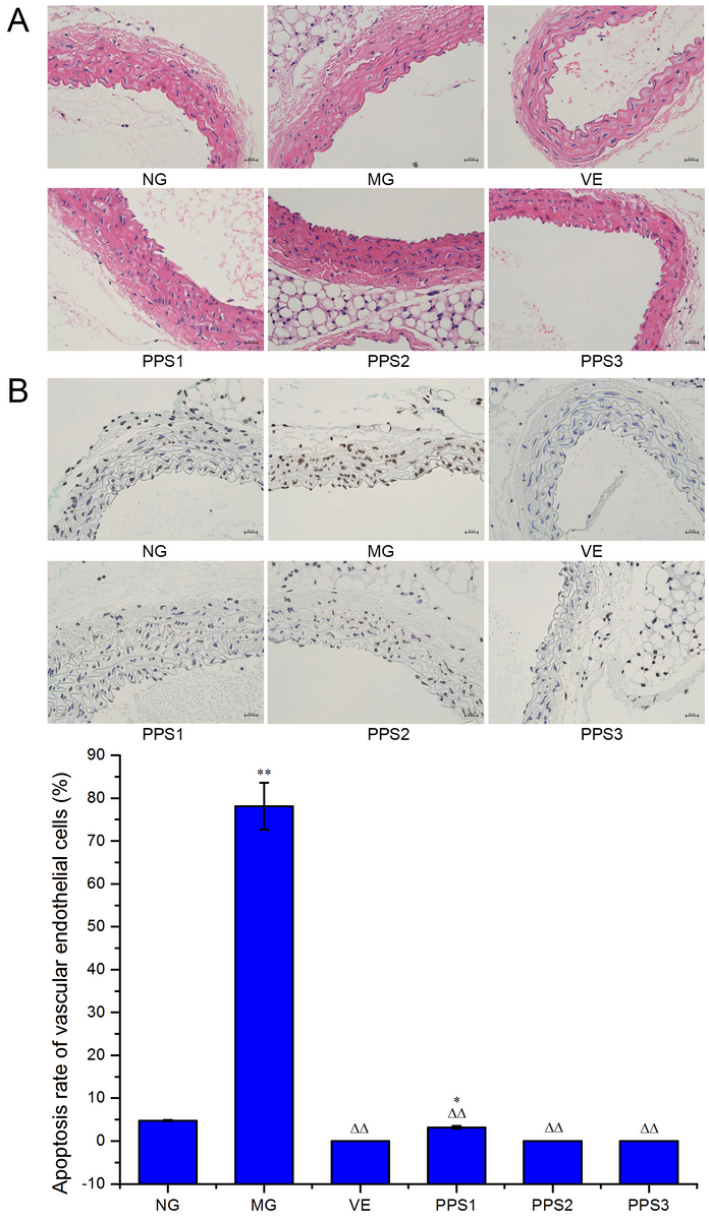

Figure 4

Representative images of HE staining (A) and TUNEL staining (B) of the mice abdominal aorta sections (× 400). NG, normal group; MG, model group, mice treated with D-galactose alone (100 mg/kg/day, ip) for 60 days; VE, positive control group, mice treated with VE (200 mg/kg/day, ig) and D-galactose (100 mg/kg/day, ip) for 60 days; PPS1, PPS2 and PPS3, mice respectively treated with 50, 100 or 200 mg/kg/day PPS (ig) and D-galactose (100 mg/kg/day, ip) for 60 days. Compared with the normal group, $*P < 0.05$, $**P < 0.01$; compared with the model group, $^{\Delta\Delta}P < 0.01$

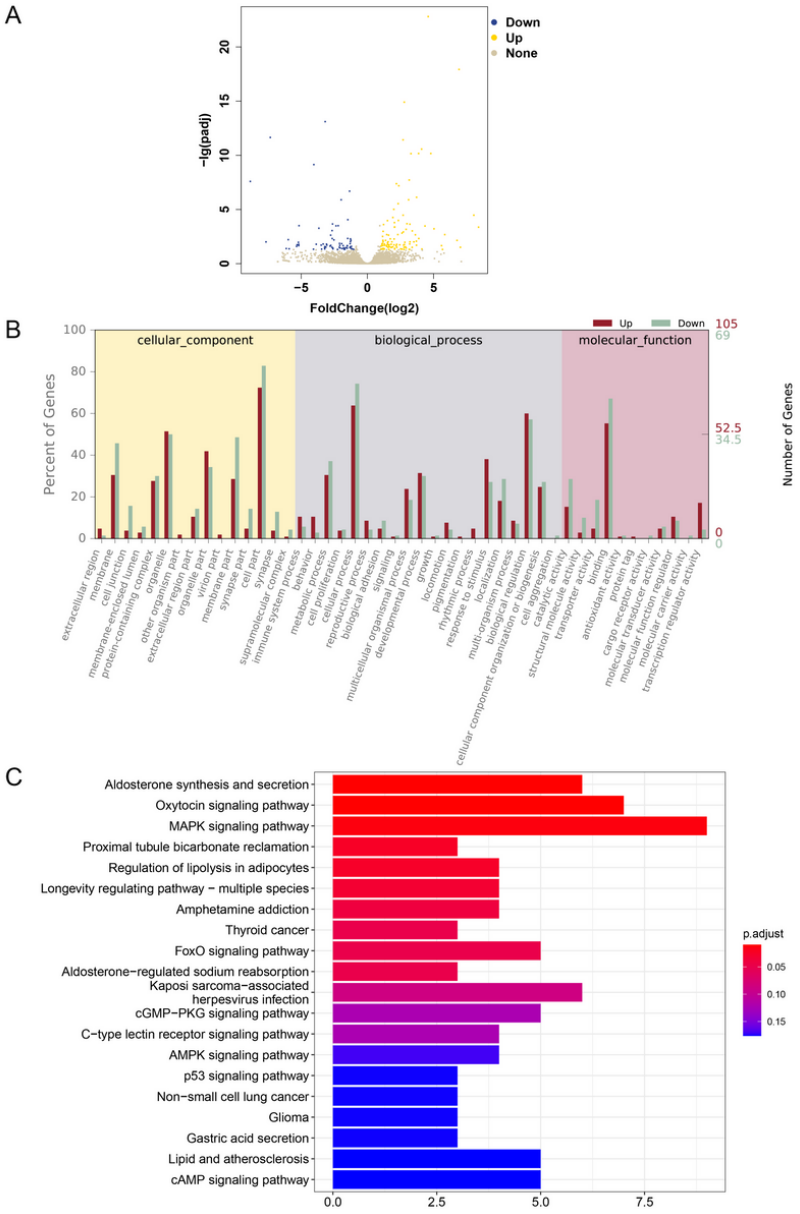

Figure 5

Effect of PPS on genes in mice abdominal aorta, compared with the model group (MG). A, volcano plots of differentially expressed genes; B, GO analysis of differentially expressed genes; C, KEGG pathway analysis of differentially expressed genes. The figures were representative of three independent experiments

Supplementary Files

This is a list of supplementary files associated with this preprint. Click to download.

- SupplementaryFig.S1.doc
- SupplementaryFig.S2.doc
- SupplymentaryFig.S3.anno.zip
- SupplementaryFig.S4.doc